EnRSim - A simple calculation tool for renewable based heating networks plant

Nicolas Lamaison[1], Mathieu Vallée[1], Jean-François Robin[1], Christine Delord[2], Romain Genet[3] and Cédric Paulus[1]

[1] CEA LITEN, Grenoble (France)

[2] INES PFE, Le Bourget du Lac (France)

[3] INDDIGO, Chambéry (France)

Abstract

Renewable-based production plants for District Heating Networks (DHN) should be deployed massively in the coming years. The present document introduces to the community a new pre-feasibility study tool, ENRSIM, to simulate such plants. That business-oriented tool allows the simulation of plants with up to 3 different units with an optional thermal storage. The plant model is implemented in Dymola and controlled using field-based expert laws using a co-simulation platform. Computation is performed over 1 year at a time step of 1 hour and takes about 1 minute on a standard laptop. An example including solar, biomass, gas and storage is here presented highlighting the type of results obtained. The example is extended to predictive control highlighting that the latter associated to MILP programming leads to optimal interactions between the components. A minimal increase of 4.3% in renewable energy content and 77% in biomass boiler startups was obtained using predictive control as opposed to field based expert laws.

Keywords: Simplified simulation tool, DHN, Renewable-based production plants, Predictive Control, MILP

1. Introduction and tool features

Due to their ability to distribute large amount of renewable energy, District Heating Networks (DHN) are expected to exhibit a considerable development in the coming years in France (DGEC France, 2019). In that context, the appropriate sizing of the renewable-based production units in accordance to the other production units becomes a prime objective. Traditional sizing methods are static and combine the demand monotone together with linear cost characteristic to obtain a break-even diagram (Frederiksen and Werner, 2013). The latter results in a piling of the heat generators on the demand monotone as a function of their profitability zones, which depend on their hours of operation. Another solution is to use dynamic tools (such as EnergyPRO®) and successive calculations.

The ENRSIM software, introduced by the present paper and cofounded by the French Renewable Energy Agency (ADEME), aims at providing such a simple dynamic tool for multi-renewable based DHN plants simulations, particularly for the integration of solar energy and storage. It targets mostly engineering offices and collectivities. It is available in French and English. The user can simulate up to 3 generators in the following list: Solar thermal, Biomass boiler, Gas boiler, CHP and Heat pump. Daily storage common to all generators and dedicated daily storage for each solar field can be setup. Finally, various configurations (serial and parallel) can be simulated. As the tool focuses on solar thermal, many parameters are available for the solar plant while the other heat units have a limited number of parameters.

Operational performances of complex energy systems can be significantly underestimated when rule-based (expert laws) control is used (Giraud et al., 2017). Thus, appropriate sizing of storage capabilities is sub-optimal when using tools based on such rules. The reasons are: i) they do not consider a time horizon compatible with the storage time constant and ii) they pre-assume specific utilization of the storage. Thus, an extension of the EnRSim calculation core to predictive control associated to Mixed Integer Linear Programming (MILP) is here presented on a case study.

The present paper is organized as follows: presentation of the EnRSim tool architecture in Section 2, a tool demo through a case study in Section 3, an extension of the case study with the introduction of predictive control in Section 4 and conclusions and perspectives in Section 5.

doi:10.18086/eurosun.2020.02.03 Available at http://proceedings.ises.org

2. Tool architecture and description

2.1. Overall architecture

Fig. 1 presents the tool architecture including a graphical user interface, pre-processing modules, the calculation core and post-processing modules. The tool performs a 1-year simulation at a time step of 1 hour. The following paragraphs give details on the pre-processing modules, calculation core and post-processing modules while the next section presents snapshot of the graphical user interface through a case study.

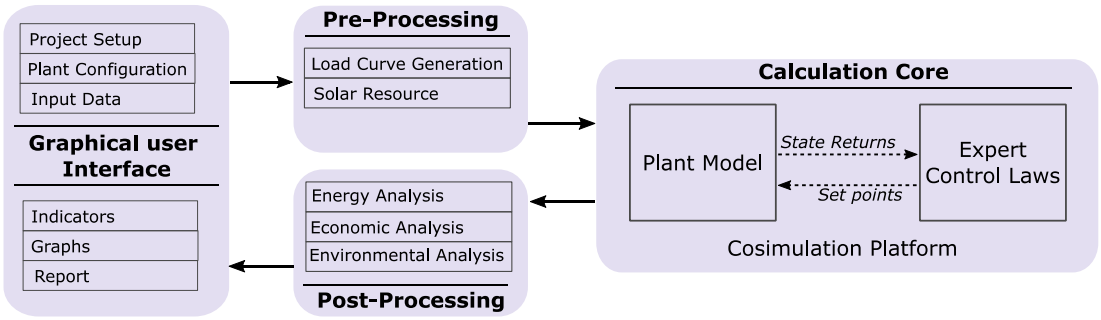

Fig. 1: Overall EnRSim tool architecture

2.2. Pre-processing modules

The first pre-processing module, referred as 'Load Curve Generation' in Fig. 1, calculates the hourly aggregated DHN heat demand and associated departure/return temperatures based on user input monthly overall heat demands. To do so, the module i) first, distributes the monthly loads among monthly losses, domestic hot water (DHW) and space heating and ii) second, allocates the calculated monthly contribution for each 1 hour time step. For both steps, the module uses the user chosen hourly ambient temperature profile together with assumptions on i) heating laws for the network temperatures, ii) yearly heat loss, iii) cold water mains temperature, iv) normed monthly distribution of DHW load, v) DHW production temperature and simultaneity factor, vi) normed daily distribution of DHW and space heating loads. The methodology implemented in this module was previously validated using real DHN data (Provent et al., 2013). It is worth mentioning that the user can also use his own load curve.

The second pre-processing module, referred as 'Solar Resource' in Fig. 1, treats the user input solar resource with i) tilt and ii) solar masks correction. The former transforms the user input horizontal direct and diffuse irradiation into the associated tilted contributions. The latter accounts for external and array shading, whose validations are respectively shown in Fig. 2 and Fig. 3 for the direct part of the irradiation (diffuse part not shown). Both figures present the value of the correction factor along the year (time step of 1 hour) in a plan Elevation vs Azimuth. For the external shading, Fig. 2 clearly shows that the external correction factor $f_{dir,e}$ is 0 (i.e. incoming irradiation is fully shaded) when the sun is below the external mask while it is 1 (i.e. no shading) when above. Regarding array shading (Fig. 3), simulations with type 56 of TRNSYS® were performed for fixed solar azimuth values (vertical lines with triangle markers on Fig. 3), which allowed validating the results obtained with the 'Solar Resource' module for the array shading correction factor $f_{dir,a}$ (circle markers).

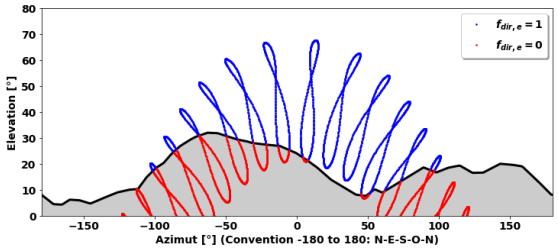

Fig. 2: 'Solar Resource' module external shading validation

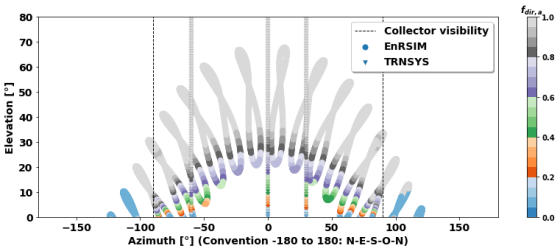

Fig. 3: 'Solar Resource' module array shading validation

2.3. Plant Model

The plant model is programmed using the Modelica language and implemented within Dymola®. It uses production unit and storage models from the in-house 'DistrictHeating' library (Giraud et al., 2015). Fig. 4 shows a schematic of the model implemented. It is meant to be generic, i.e. the goal is to have a single model capable of

managing a large majority of the current configurations or ones that look promising going forward for a heating network thermal plant. In this thermal heating plant model, we find 5 potential generators in parallel (Biomass, Cogeneration, Heat Pump, Gas and Solar), 3 potential generators in series upstream (Cogeneration, Heat Pump, Solar), 1 potential common storage and 1 back-up generator whose aim is to satisfy the load curve in all circumstances. Both solar fields also include a dedicated storage. For each of the block embedded, steady-state mass balance and dynamic energy balance are solved. Further details are provided in Appendix.

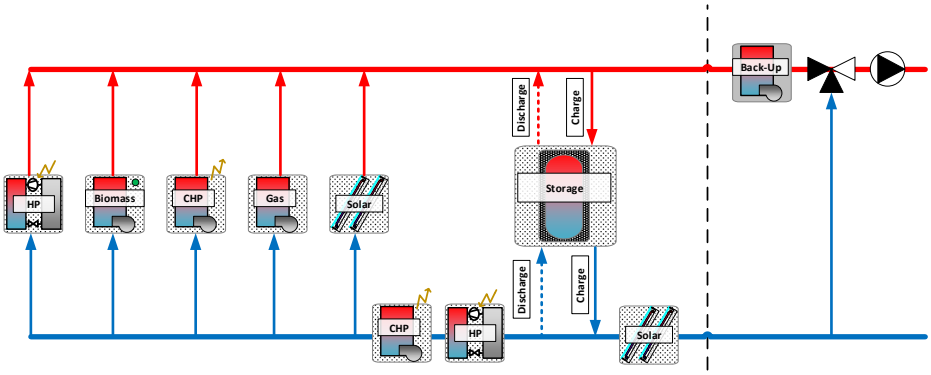

Fig. 4: Schematic of the generic calculation core plant model

The Modelica-based plant model is encapsulated using FMI standard (FMI development group, 2014) and embedded into the in-house co-simulation platform PEGASE (Vallée et al., 2019) where it is operated aside a controller module containing the expert laws. Fig. 1 illustrates the interaction between the plant model and the controller.

2.4. Expert Control Laws

The EnRSim tool is based on predefined control laws. The parameters of each unit for the control laws are i) the calendar availability (A), ii) the priority (P), iii) the minimum and maximum thermal power (P_{min}/P_{max}), and iv) the maximum outlet temperature ($T_{o,max}$). Depending on the plant configuration (2 units in parallel and 1 unit in upstream serial, 3 in parallel, 2 in serial, etc.) , the control laws are different. Fig. 5 presents the expert law logic for 2 units in parallel. Each branch leads to a set of thermal power and mass flow rate set points for both generators. Startup and shutoff are handled within this logic diagram.

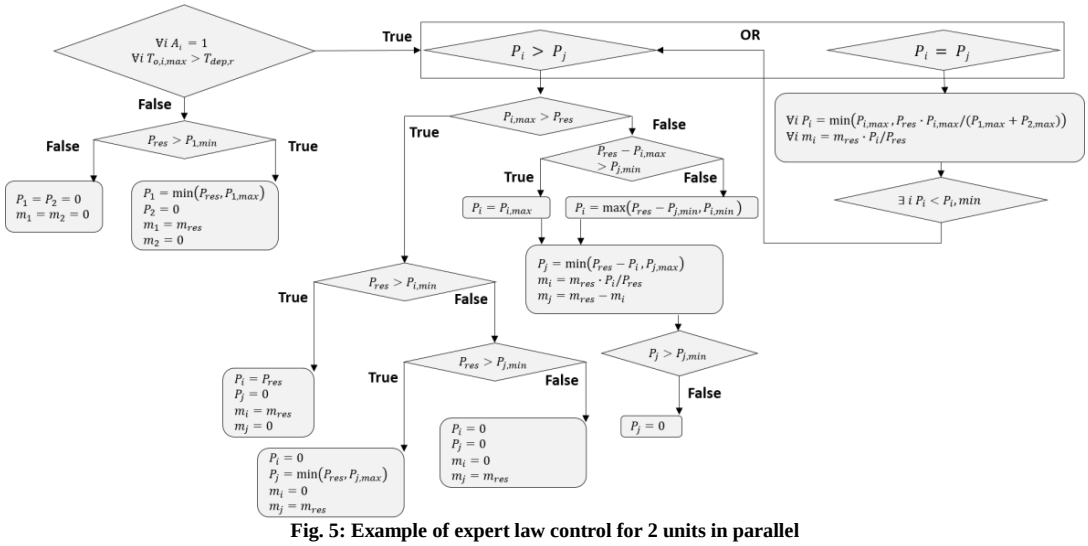

Fig. 5: Example of expert law control for 2 units in parallel

Another set of control laws exist for the common storage (shown in Fig. 4). For the latter, the user can choose between 'Charging' or 'Discharging' priority. For both priorities, charge and discharge modes are controlled differently, as shown in Fig. 6, depending on the storage state of charge (τ) and the level of thermal power of each generator (P_i). To summarize, charging priority prevents frequent start and stop of generators while discharging priority favors storage discharge during peak demand events.

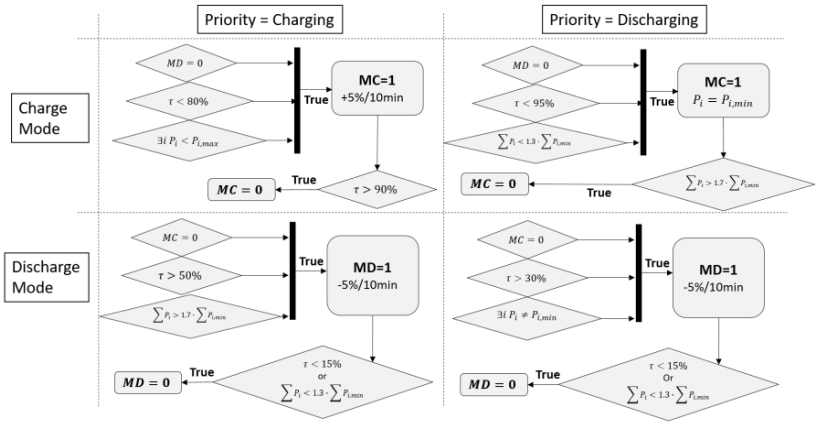

Fig. 6: Common storage expert control laws

2.5. Post-processing modules

The tool includes three post-processing modules that respectively calculate economic (e.g. Levelized Cost of Heat), energetic (e.g. Solar fraction), technical (e.g. number of startups) and environmental indicators (e.g. CO2 emissions and renewable energy ratio).

3. Case study

This section introduces the case study addressed in the present paper. The case study is first used to present snapshot of the tool graphical user interface (see section 3). Second, it is used to compare expert control and predictive control (see section 4).

3.1. Presentation

The architecture chosen for the present case study is shown in Fig. 7, which is a snapshot of the plant configuration tab of the tool graphical user interface (GUI). This architecture represents a typical problem of solar thermal integration into district heating network production plants already equipped with a biomass boiler. In such a case, the biomass boiler generally operates as base load generator during the heating season and is stopped during summer because of minimum load technical constraint. In summer, the gas boiler thus ensures the entire load. In order to increase the summer renewable energy share, solar thermal seems to be an attractive solution.

However, this solution is problematic during mid-season when the biomass is still operating. Indeed, the solar thermal production during sunny days of the mid-season may push the biomass boiler close to its technical minimal load and sometimes even to stoppage. The latter leads to significant operational difficulties and generally results unwantedly in an increase of gas share in the production mix. The use of a storage can reduce this behavior. However, its sizing and control operation represent tedious tasks.

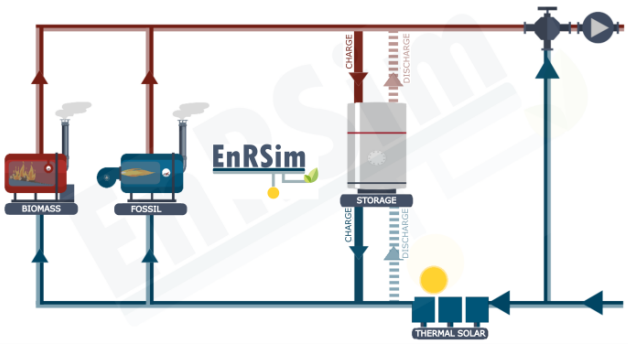

Fig. 7: Plant Configuration Tab

For the present case study, the solar field has an upwind serial position with respect to the biomass boiler, gas boiler and storage, as seen in Fig. 7. With this location, the solar field is not affected by possible higher temperature coming from the storage during charging phase. However, the solar field does not have access to the common storage and must then be equipped with a dedicated storage (not shown on Fig. 7). In this position, the common storage is thus useful to the biomass boiler operation only.

Lyon (France) was chosen as the location of the production plant. From weather data from MeteoNorm®, the 'Load Curve Generation' pre-processing module (see section 2) constructed the load curves, whose GUI snapshots

are shown in Fig. 8 and Fig. 9, respectively for the thermal power monotone and the hourly DHN temperature variations.

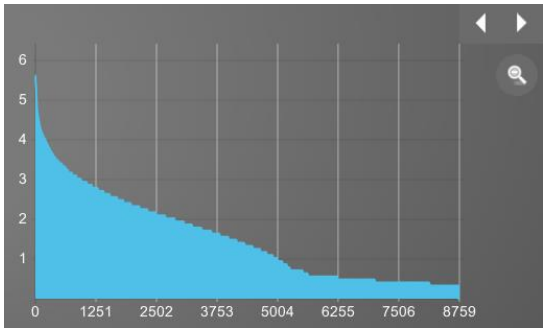

Fig. 8: Monotone of the load curve (MW)

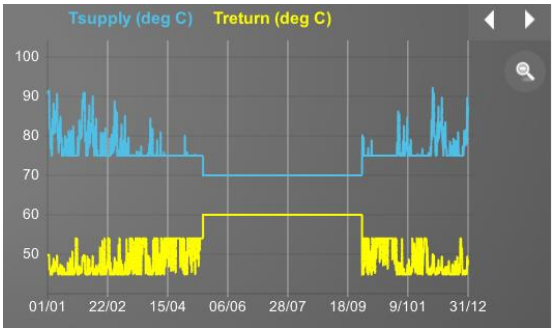

Fig. 9: Generated Load Curve (Temperatures)

The base sizing considered for this production plant is as follows:

- Common storage : 400m^3 (about 22MWh for the DHN operational temperatures, see Fig. 9) ;
- Solar field: 150 solar collectors of about 15m² each of transparent area whose characteristics are typical of large collectors designed for district heating applications. The solar collectors azimuth and tilt are respectively 0° and 30°. As explained beforehand, a solar field dedicated storage of 100m^3 is also considered, the storage operating as an interface between the solar field and the network return pipe;
- The biomass boiler nominal power is 4.5MW with a minimum to maximum power ratio of 30%. The biomass is stopped during summer season (from 15th of May to 1st of October).

The solar thermal field is operated at constant primary (solar collectors) and secondary (between heat exchanger to storage) flow rates. The latter is set to induce a 20K temperature increase throughout the field at the field nominal power ($700 \cdot A_{solar,field}$ with $A_{solar,field}$ $[m^2]$ the total solar field transparent area). The flow rate from the DHN through the storage depends on the temperature level in the storage. When the latter is below the return temperature of the DHN, the flow rate is set to zero. When it is above the DHN return temperature but below the DHN departure temperature, it is set equal to the DHN flow rate. Finally, if it is above the departure temperature, flow mixing is performed as shown in Equation (1).

$$\dot{m}_{sol} = \dot{m}_{DHN} \cdot \frac{T_{dep,DHN} - T_{ret,DHN}}{T_{high,stock} - T_{ret,DHN}} \quad (1)$$

With $\dot{m}_{sol}$ $[kg/s]$ and $\dot{m}_{DHN}$ $[kg/s]$ the flow rates respectively through the solar dedicated storage and the DHN, and $T_{dep,DHN}$, $T_{ret,DHN}$ and $T_{high,stock}$ the DHN departure, DHN return and top solar dedicated storage temperatures.

3.2. GUI results

Fig. 10 and Fig. 11 present snapshots of the GUI results visualization panel with respectively a zoom of the hourly production trajectories and the monthly energy mix. In addition to those results, the GUI provides a set of indicators and alerts regarding undesired results (solar field overheating, high number of generator startups, etc.). Finally, the user can generate an automatic report with an extra set of graphs.

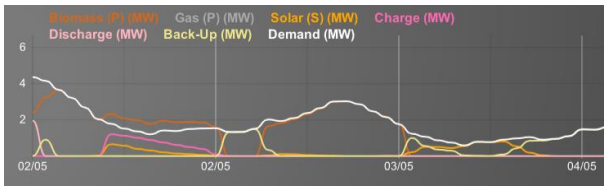

Fig. 10: Production trajectories

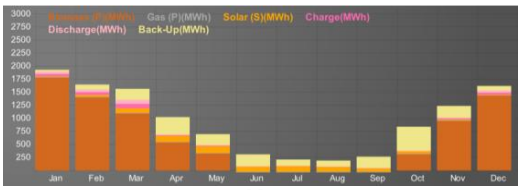

Fig. 11: Monthly Energy Mix

For the base sizing of the case study, the results listed in the GUI are an energy mix composed of 74.2% biomass, 9.8% solar and 16.0% gas. The number of biomass startup is however very high (177) and the tool thus gives an alert. At this point, it is worth mentioning that number of startup includes both cold and warm startup. While the former represents switch off of the generator for a long period of time, the latter represents short switched off periods. For the biomass boiler, it means that it does not produce for the DHN but its combustion chamber is kept at nominal temperature.

Further results will be shown in the next section, which will compare various sizing but also various control laws.

4. Sizing influence and extension to predictive control

The present section will deal with simulations of the case study for various sizing of the biomass boiler. In addition, we will show the influence on the sizing of the substitution of expert laws by predictive control.

4.1. Principles of predictive control

During the sizing stage, representative boundary conditions (weather, loads, etc.) over a given temporal horizon are generally supposed. Accounting for the knowledge of this boundary conditions in the future ($t > t_{now}$) when taking an operation decision at time t_{now} gives a predictive rather than reactive characteristic to the controller. The principle of predictive control is thus to benefit from previsions on boundary conditions by evaluating their impact on the future states of the system and including this knowledge in the calculation of next operational set points.

Accounting for the knowledge of the future boundary conditions using an expert law (i.e. rule-based) approach can be very complex to formulate and is generally sub optimal. Another solution is to use a mathematics-based approach in which the physic of the production plant is described in a simplified manner within a mixed integer linear programing (MILP) framework. The latter allows accounting for system-based constraints (mass and energy balances) together with technical constraints (power levels, ramps, etc.) in the calculation of the control trajectories while certifying an optimal of an objective function (generally the cost) with respect to the constraints defined. The combination of predictive control and MILP is referred from now on as optimal control.

The general MILP formulation is shown in Equation (2). The objective is to find the vector of decision variables $\boldsymbol{x}^T = (\boldsymbol{x_1}, \dots \boldsymbol{x_j}, \boldsymbol{x_{j+1}}, \dots, \boldsymbol{x_n})$ solution of the problem of Equation (2), $\boldsymbol{x}$ being composed of continuous $(1, \dots, j)$ and integer $(j+1, \dots, n)$ variables.

$$\min_x f_{cost} = c^T.\boldsymbol{x} \quad with \begin{cases} LHS \leq A.\boldsymbol{x} \leq RHS \\ l_b \leq \boldsymbol{x} \leq u_b \end{cases} \tag{2}$$

where c [n] is a vector of cost, A[m x n], LHS[m] and RHS[m] are respectively the matrix and vectors of linear constraints, and l_b [n] and u_b [n] are respectively the lower and upper bounds vector for the decision variables.

Fig. 12 presents the modifications operated to EnRSim calculation core (see Fig. 1) in order to integrate optimal control as a replacement of expert law reactive control. The modifications are two folds:

i) The new temporal scheme with consideration of the boundary conditions over the horizon t to $t + future$. It is worth mentioning here that $future$ means a given number of time steps (48 for the present case study). The latter allows having a tractable MILP problem that can be solved rapidly. In order to perform a simulation, we perform an optimization over the next 48 hours at every time step of 1 hour. That temporal scheme is referred as receding horizon with the end of the $future$ number of time steps getting closer and closer to the end of the year at each simulation. The PEGASE co-simulation platform (Vallée et al., 2019) which embeds the calculation core has native receding horizon capabilities.

ii) The replacement of the rule-based reactive control block by the optimal block whose equations are described in next section.

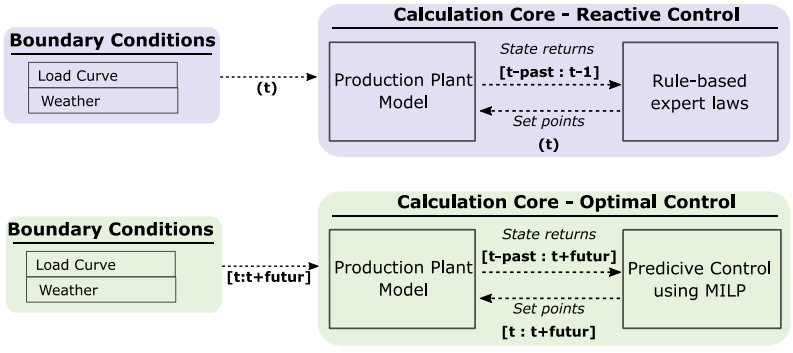

Fig. 12: Extension of EnRSim calculation core to optimal control

4.2. MILP model

The different models used for the MILP formulation of the case study are now described. In the following equations, the bold variables represent optimisation variables, i.e. the ones constituting the $\boldsymbol{x}$ vector from equation (2).

Equation (3) : System energy balance

In the energy balance of Equation (3), the thermal power of he biomass boiler $\left(\boldsymbol{P^{bio}}(t)\right)$, gas boiler $\left(\boldsymbol{P^{gas}}(t)\right)$, and charge/discharge ($\boldsymbol{P^{st}_{charge}}(t)$ and $\boldsymbol{P^{st}_{discharge}}(t)$) of the storage are optimization variables. The total demand (P_{load}) is a boundary condition while the solar production (P^{sol}), calculated by the plant production model at each time step of the future horizon, is an input data.

$$\boldsymbol{P^{bio}}(t) + \boldsymbol{P^{gas}}(t) + \boldsymbol{P^{st}_{décharge}}(t) + P^{sol}(t) = \boldsymbol{P^{st}_{charge}}(t) + P_{load}(t) \quad (3)$$

Equation (4) : Heat generators power levels constraints

Equation (4) is used for both the biomass and gas boilers. r^i represent the ratio betwenn the minimum and nominal power P^i_{max} of generator 'i' (30% and 0% respectively for the biomass and gas boiler). $\boldsymbol{P^i}(t)$ is the thermal power of generator 'i' and $\boldsymbol{Y^i}(t)$ represent the state ON (1) or OFF (0) of generator 'i'.

$$r^i * P^i_{max} * \boldsymbol{Y^i}(t) \leq \boldsymbol{P^i}(t) \leq P^i_{max} * \boldsymbol{Y^i}(t) \quad (4)$$

Equations (5) and (6) : Heat generators startup constraints

In order to be representative and avoid unrealistic heat generators startup at high frequency, it is necessary to constrain it by introducing a new intermediate variable $\boldsymbol{X^i}(t)$. The latter is 1 when the generator is started and 0 the rest of the time, as shown in Equation (5). Equation (6) is then used to set the value of $\boldsymbol{X^i}(t)$. However, the latter equation does not set the value of $\boldsymbol{X^i}(t)$ when $\boldsymbol{Y^i}(t-1) = \boldsymbol{Y^i}(t) = 1$, i.e. when the generator is ON and stays ON (a very frequent situation). In this situation, we want the value of $\boldsymbol{X^i}(t)$ to be 0. Introducing startup costs in the objective function (see Equation (12)) will force the optimizer to use $\boldsymbol{X^i}(t) = 0$ in this situation.

$$\boldsymbol{X^i}(t) = \begin{cases} 1 \; if \; \boldsymbol{Y^i}(t-1) = 0 \; and \; \boldsymbol{Y^i}(t) = 1 \\ 0 \; however \end{cases} \quad (5)$$

$$\boldsymbol{Y^i}(t) - \boldsymbol{Y^i}(t-1) \leq \boldsymbol{X^i}(t) \leq \boldsymbol{Y^i}(t) \quad (6)$$

Equations (7) to (11): Storage model

Equation (7) present the energy balance of the storage with $\boldsymbol{P}$ $[W]$ and $\boldsymbol{E}$ $[J]$ respectively the power and energy, Δt[s] the time step, K_{loss} $[s^{-1}]$ the heat loss coefficient and the indices 'ch' and 'disch' for charge and discharge. Equation (8) sets equal the storage energy at time $t = 0$ and $t = t_{future}$, which corresponds to the end of the future horizon considered by the optimal control. Equations (9) and (10) represent the thermal power limit (P^{st}_{max}) for the charge and discharge with $\boldsymbol{Y^{st}}$ a binary variable forcing the storage to be either charging or discharging but never both at the same time. Finally, Equation (11) limits the maximum of energy E^{st}_{max} that the storage can handle.

$$\frac{\boldsymbol{E^{st}}(\boldsymbol{t}) - \boldsymbol{E^{st}}(\boldsymbol{t-1})}{\Delta t} = \boldsymbol{P^{st}_{ch}}(\boldsymbol{t}) - \boldsymbol{P^{st}_{disch}}(\boldsymbol{t}) - K_{loss} * \boldsymbol{E^{st}}(\boldsymbol{t}) \quad (7)$$

$$\boldsymbol{E_{st}}(\boldsymbol{t=0}) = \boldsymbol{E_{st}}(\boldsymbol{t = N \cdot \Delta t}) \quad (8)$$

$$0 \leq \boldsymbol{P^{st}_{ch}}(\boldsymbol{t}) \leq P^{st}_{max} * \left(1 - \boldsymbol{Y^{st}}(\boldsymbol{t})\right) \quad (9)$$

$$0 \leq \boldsymbol{P^{st}_{dech}}(\boldsymbol{t}) \leq P^{st}_{max} * \boldsymbol{Y^{st}}(\boldsymbol{t}) \quad (10)$$

$$0 \leq \boldsymbol{E^{st}}(\boldsymbol{t}) \leq E^{st}_{max} \quad (11)$$

Equation (12): Objective function

The objective function for the MILP model is shown in Equation (12). The latter is composed of startup c^i_{dem} and production c^i_{prod} costs for each generator 'i'. The variable Hor is the number of time steps of the horizon considered and N_{equ} is the number of generator (2 in the present case study). The starting costs of the biomass boiler are here considered 3 times higher than the gas boiler ones.

$$f_{cout} = c_{dem} + c_{prod} = \sum_{t=1}^{Hor} \sum_{i=1}^{N_{equ}} c_{dem}^{i} * \boldsymbol{X^i}(t) + \sum_{t=1}^{Hor} \sum_{i=1}^{N_{equ}} c_{prod}^{i} * \boldsymbol{P^i}(t) * \Delta t \quad (12)$$

The MILP model has been implemented using an in-house library. At each time step, the MILP model is solved using Cplex (IBM ILOG, 2015).

4.3. Results

Fig. 13 presents a synthesis of the results obtained for the case study (biomass boiler, gas boiler, storage and solar thermal field, see Section 3). The biomass nominal power is varied from 2 to 6MW while the rest of the parameters and sizing are kept fixed. Rules-based (expert law) and optimal control are compared. The results are shown in a plan Yearly gas share =f(number of biomass startup). The number of full storage cycles (i.e. ratio of the yearly integral of charged power over maximum storage energy) is also shown with a color scale.

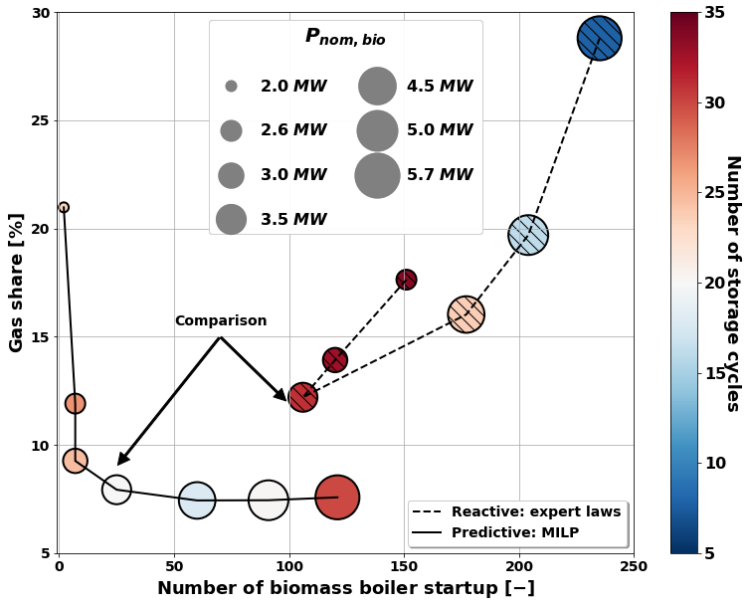

Fig. 13: Gas share as a function of number of biomass boiler startup for various size of biomass boiler – Expert laws vs predictive control

The main conclusions to draw from Fig. 13 are the following:

- For all the cases, the optimal control allow limiting both the gas share and the number of biomass startup with respect to the expert laws;
- The obtained results are much more sensitive to the biomass boiler sizing in the case of the expert laws;
- The expert law control presents an optimum with respect to the 2 indicators (for $P_{nom}^{bio} = 3.5MW$) while the predictive control presents a Pareto front, i.e. for each point of the curve, there is no other point for which both indicators are better. This fact highlights clearly that optimal control reaches control optimality for each design;
- For the expert laws, the increase of biomass startup below a sizing of 3.5MW is due to the static laws presented in section 2. Indeed, the storage discharge is stopped based on the power level at a given time instant and a margin with respect to the minimum power. The latter gives a smaller margin when the minimum power of the biomass is smaller. The solar production being the same, this margin is not sufficient anymore to prevent a stoppage of the biomass boiler, i.e. storage discharge is too significant;
- Finally, the non-adaptive feature of the expert laws leads to a monotonic storage cycles variations when the biomass boiler sizing is decreased. Contrarily, the adaptive feature of the optimal control modify its storage behavior as a function of the biomass boiler sizing, leading to non-monotonic storage cycles evolution.

Thus, Fig. 13 shows clearly a strong inter-dependency between the sizing optimization and the expert law parametrization. However, using optimal control allows focusing on the optimization of the sizing with respect to a set of indicators without having to readjust for each sizing the parameters of the controller. The 2 systems pointed out by an arrow on Fig. 13 are now studied with more details (Pmax/Pmin = 3.5MW/1.05MW).

Fig. 14 and Fig. 15 presents the daily averaged monotone of the demand together with the associated energy mix respectively for expert law and predictive control. The striking result here is the better storage usage during the critical periods, i.e. during winter peaks and mid-season solar intermittency, when using predictive control. The latter leads to an extra gas usage when using expert laws during these critical periods.

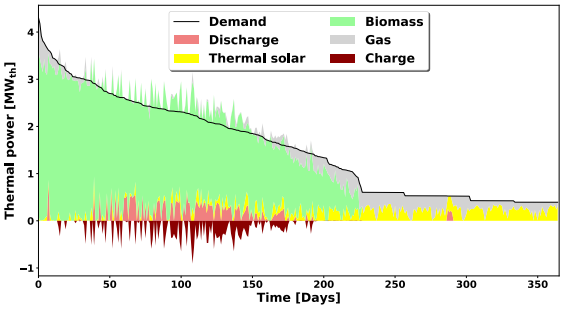

Fig. 14: Daily averaged monotone of the demand and energy mix for expert laws control ($P_{nom}^{bio} = 3.5MW$)

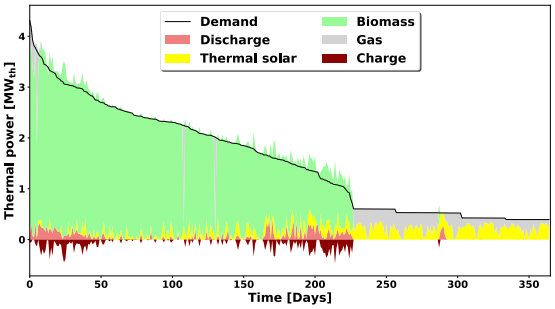

Fig. 15: Daily averaged monotone of the demand and energy mix for predictive control ($P_{nom}^{bio} = 3.5MW$)

In view of this advantageous storage behavior with optimal control, the energy mix is more virtuous, as shown in Tab. 1 with 4.3% increase in renewable energy content of the production. Additionally, the number of biomass startup is reduced by 77%. It is worth noticing here that, when looking at Fig. 13, those values represent the lower boundaries of the benefit we can obtain with optimal control. Thanks to optimal control, the initial willingness, which was increasing the renewable energy share in summer by integrating solar thermal, can thus be achieved without introducing control issues during mid-season.

It is worth mentioning here that we have performed our analysis with a fixed solar thermal field and common storage size with only a variation of the biomass boiler size. A different approach with a fixed biomass boiler size but varying solar field size would have led to a larger solar field using optimal control for the same set of indicators.

Tab. 1 : Energy mix and number of biomass boiler startup obtained for the sizing $P_{nom}^{bio} = 3.5MW$

	Expert Laws	Optimal Control
Biomass [%]	78.0	82.3
Thermal solar [%]	9.8	9.8
Gas [%]	12.2	7.9
Renewable Energy Content [%]	87.8	92.1
Number of biomass boiler startup [-]	106	25

A closer look on the operational differences between the 2 control modes is presented in Fig. 16 and Fig. 17. The figures highlight 5 days of operation early May, i.e. mid-season, respectively for expert laws and predictive control. Both the energy mix and the storage level are shown on the 2 graphs. Interestingly, the storage is much more active when using expert laws with an overall very high storage level. However, the expert laws are i) unable to discharge the storage to avoid using gas during the first demand peak above the nominal biomass boiler power and ii) unable to charge the storage during the solar production toward the end of the week, leading to undesired biomass stoppages. Optimal control however leads to no gas consumption during these 5 days of operation. It is also worth noting that in this control mode the charge and discharge phases are arranged so that heat does not stay too long in the storage. The latter is due to Equation (7) and the heat loss associated to high level of energy is the storage. The optimizer will always try to limit them.

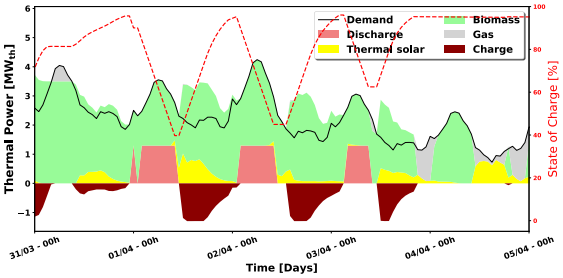

Fig. 16: Detailed hourly results for 5 days in April and expert laws control ($P_{nom}^{bio} = 3.5MW$)

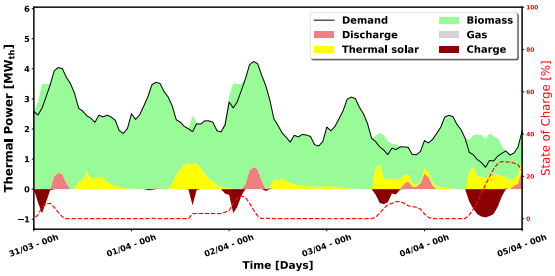

Fig. 17: Detailed hourly results for 5 days in April and predictive control ($P_{nom}^{bio} = 3.5MW$)

5. Conclusion and perspectives

The present paper introduced the EnRSim tool, a simulator of renewable-based production plants using field-based expert laws. That tool aims at helping professionals to size the units in the pre-feasibility stage. The tool is composed of i) pre-processing modules calculating the DHN load and the solar resource corrections, ii) a calculation core based on a co-simulation platform including a model of the production plant and a rule-based control module, iii) post-processing modules for energetic, economic and environmental calculations, iv) a user friendly graphical user interface, and v) an automatic report generation engine. Up to three generators among biomass boiler, solar thermal, heat pump, cogeneration and gas boiler can be simulated in various configuration (serial and parallel) with or without storage. Yearly simulations are performed at a time step of 1 hour in about 1 minute on an office laptop computer. A case study using biomass boiler, solar thermal field, gas boiler and storage showed the type of results obtained, i.e. production trajectories and key performance indicators. Since summer 2020, the tool including expert law control is available for download in French and English for free.

The EnRSim calculation core was then modified by replacing the expert law control block with optimal control (predictive control with MILP model and receding horizon). The paper then shows how optimal control can be used in a sizing stage. The same case study as for the tool demo was extended to various biomass boiler sizing and tested under optimal and expert law controls. In summary, the advantage of predictive control combined to MILP is that the interactions between the components of the production plant are not predefined and are rather calculated optimally and at each time step. The latter allows the controller to be adaptive and led for the case study to a minimal 4.3% increase in renewable energy content and 77% reduction in biomass boiler startup. With such an approach, the full potential of a storage can thus be accounted for in sizing stage. More specifically, it is shown here that for the MILP, the storage handles more properly both the peak heat demands in winter and the potential short biomass startup/shutoff cycles in mid-season. There is obviously the possibility of improving both the expert law and its parameters. Better results, but not better than the MILP (for which optimality is proven), should be obtained at the price of a time-consuming iteration process to find the right set of parameters, which itself depends on the sizing and thus require an update for each sizing.

The extension of EnRSim calculation core to predictive control will allow evaluating more profitably additional configuration combining biomass, solar thermal and storage, especially those for which the common storage can also be used by the solar field, as done in many existing installations.

6. Acknowledgments

The authors wish to thank ADEME, the French Renewable Energy Agency, for its co-funding for the EnRSim project. The EnRSIM tool is available for download at the following link: **https://enrsim.ines-solaire.org.**

7. References

FMI development group, 2014. Functional Mock-up Interface for Model Exchange and Co-Simulation 2014. [WWW Document]. Httpsfmi-Stand.-Dev. URL (accessed 3.25.20).

Frederiksen, S., Werner, S., 2013. District Heating and Cooling. Professional Pub Serv.

Giraud, L., Bavière, R., Vallée, M., Paulus, C., 2015. Presentation, Validation and Application of the DistrictHeating Modelica Library. Versailles, France, p. 10. https://doi.org/10.3384/ecp1511879

Giraud, L., Merabet, M., Baviere, R., Vallée, M., 2017. Optimal control of district heating systems using dynamic simulation and mixed integer linear programming, in: Proceedings of the 12th International Modelica Conference, Prague, Czech Republic, May 15-17, 2017. Linköping University Electronic Press, pp. 141–150.

IBM ILOG, 2015. IBM ILOG CPLEX Optimization Studio V12.7.0 documentation.

Provent, A.-S., Guillot, B., Renaude, F., Dumas, J., Genet, R., Martins, M., Le Denn, A., 2013. Smart Grid Solaire Thermique: Rapport d'étude sur les réseaux de chaleur existants et les réseaux adaptés aux Eco-quartiers (No. 1.1.1). ADEME.

Vallée, M., Bavière, R., Seguin, V., Vuillerme, V., Lamaison, N., Descamps, M., Aurousseau, A., 2019. An efficient co-simulation and control approach to tackle complex multi-domain energetic systems: concepts and applications of the PEGASE platform. Presented at the ECOS conference, Wroclaw, Poland.

Appendix: Details of the dynamic plant models

Biomass, Gas and CHP

From the point of view of the core calculation, biomass, gas and cogeneration generators are modelled in the same way. It is important to note that in this model, we consider only the power injected in the heat transfer fluid. The difference in yield between these generators is calculated in the post-processing. Another difference between these models is in the user's settings.The energy balance for this model of generator is presented in equation (13) below.

$$\left((\rho.cp.V)_f + C_{bo}\right).\frac{dT_{out}}{dt} = P_{bo} - \dot{m}_f.cp.(T_{out} - T_{in}) - G.(T_{moy} - T_{ext}) \quad (13)$$

Where $\rho\ [kg.m^{-3}]$ is the density of the heat transfer fluid, $cp\ [J.kg^{-1}.K^{-1}]$ the heat transfer fluid's specific thermal capacity, $V\ [m^3]$ the internal volume of the combustion chamber $[m^3]$, $C_{\mathrm{bo}}\ [J.K^{-1}]$ the boiler's thermal capacity, $P_{bo}\ [W]$ the power transferred to the fluid by the boiler, $\dot{m}_f\ [kg.s^{-1}]$ the flow of the heat transfer fluid, $T_{out}\ [K]$ and $T_{in}\ [K]$ the respective inlet and outlet temperatures, $T_{moy}\ [K]$ the heat transfer fluid's mean temperature in the boiler, $T_{ext}\ [K]$ the room temperature in the boiler room and $G\ [W.K^{-1}]$ an overall thermal loss coefficient.

If these generators are installed in parallel, the settings sent by the control unit are the power and the flow. If the generators are installed in series (cogeneration), the setting sent by the control unit is only the power.

Heat pump

The energy balances for the heat pump model are presented in Equations (14), (15) and (16). The COP (coefficient of performance) laws are explained in Equation (17) and (18).

$$\rho.cp.V_{hot}.\frac{dT_{hot}^{out}}{dt} = -Q_{hot} - \dot{m}_{f,hot}.cp.\left(T_{hot}^{out} - T_{hot}^{in}\right) \quad (14)$$

$$\rho.cp.V_{cold}.\frac{dT_{cold}^{out}}{dt} = -Q_{cold} - \dot{m}_{f,cold}.cp.\left(T_{cold}^{out} - T_{cold}^{in}\right) \quad (15)$$

$$W + Q_{hot} + Q_{cold} = 0 \quad (16)$$

$$COP_{global} = -\frac{Q_{hot}}{W} \quad (17)$$

$$COP_{global} = K_{degrad}.Coeff_{carnot}.\frac{T_{hot}^{out}}{T_{hot}^{out} - T_{cold}^{out}} \quad (18)$$

Where $V_{hot}\ [m^3]$ and $V_{cold}[m^3]$ are respectively the volumes of heat transfer fluid on the hot side (condenser) and cold side (evaporator) of the heat pump, $T_{hot}^{out}\ [K]$ and $T_{cold}^{out}\ [K]$ the outlet temperatures on the hot and cold side respectively, $T_{hot}^{in}\ [K]$ and $T_{cold}^{in}\ [K]$ the inlet temperatures on the hot and cold side respectively, $\dot{m}_{f,hot}\ [kg.s^{-1}]$ and $\dot{m}_{f,cold}\ [kg.s^{-1}]$ the respective flows on the heat network and cold source sides in the heat pump, $Q_{hot}\ [W]$ and $Q_{cold}\ [W]$ the thermal power transferred to the fluid on the hot and cold side respectively, $W\ [W]$the electrical power of the heat pump compressor, $COP_{global}\ [-]$ the heat pump's coefficient of performance, $Coeff_{carnot}$ a coefficient representing the heat pump's performance relative to a Carnot efficiency (set from the man-machine interface) and $K_{degrad}\ [-]$ a linear coefficient of degradation of the COP between 0 and 1 between a heating capacity of 0 and a minimum heating capacity (given by the man-machine interface) $Q_{hot,min}\ [W]$.

If the generator is installed in parallel, the instructions sent by the control unit are the power and the flow. If the generator is installed in series, the instruction sent by the control unit is only the power.

Storage

The storage system's stratification is considered. It is therefore discretized in N_{seg} segments (see Fig. 18). The storage has an input/output port at the top and an input/output port at the bottom for the charge/discharge modes respectively.

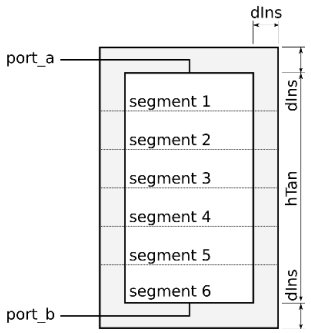

Fig. 18: Schematic of the stratified storage model

The distributed model of this sensible storage is presented in Equation (19) for each segment 'i'.

$$Q_{top,i} + Q_{bot,i} + Q_{pertes,i} = \rho . cp . V_i . \frac{dT_{out,i}}{dt} + \dot{m}_{f,st} . cp . \left(T_{out,i} - T_{out,i-1}\right) \quad (19)$$

Where $Q_{top,i}\ [W]$ and $Q_{bot,i}\ [W]$ are the thermal exchanges at the top and bottom terminals of the element considered. These thermal powers take into account i) the axial conduction between the different fluid elements, ii) the thermal loss through convection at the top and bottom of the storage and iii) an automatic destratification term if a cold element should be above a hot element. $Q_{pertes,i}\ [W]$ represents the thermal loss of segment 'i' through its lateral surface, $\dot{m}_{f,st}\ [kg.s^{-1}]$ is the flow of fluid in the storage. Lastly, V_i, $T_{out,i}$ and $T_{out,i-1}$ respectively represent the volume, the outlet temperature of segment 'i' and the outlet temperature of element 'i-1'.

Depending on how the storage is used, it is important that the $\dot{m}_{f,st}$ sign varies (positive for discharging and negative for loading). For this storage, the instruction sent by the control unit is the through flow $\dot{m}_{f,st}$.

Solar field

The energy balance in this element is presented in the Equations (20) and (21) below.

$$C \frac{dT_m}{dt} = A_{field}(\eta_0 G_T - a_1(T_m - T_a) - a_2(T_m - T_a)^2) + \dot{m}_{sol} cp (T_{in} - T_{out}) \quad (20)$$

$$G_T = I_b K_b + I_d K_d \quad (21)$$

Where $C\ [J.kg^{-1}]$ is the total capacity of the panel (fluid and structure), $T_m\ [K]$, $T_{in}\ [K]$, $T_{out}\ [K]$ and $T_a\ [K]$ the mean inlet, outlet and exterior temperatures, $A_{field}\ [m^2]$ the area of the field considered, $\eta_0\ [-]$, $a_1\ [-]$ and $a_2\ [-]$ respectively the optic effectiveness and the coefficient of first order and second order thermal losses, $\dot{m}_{sol}\ [kg.s^{-1}]$ the solar exchanger's secondary flow (network side), $cp\ [J.kg^{-1}.K^{-1}]$ the specific thermal capacity of the heat transfer fluid, $I_b[W \cdot m^{-2}]$ and $I_d[W \cdot m^{-2}]$ respectively the direct and diffuse irradiation in the collector tilt, and $K_b[-]$ and $K_d[-]$ the incidence angle modifiers respectively for the direct and diffuse radiations.

The modelling of the exchanger is done through a constant thermal conductance. The inertia and the thermal losses in the field's pipes are taken into account through thermal capacities and conductance. The modelling of the solar storage is similar to that used for the common storage system.

For the installation of this field in parallel and in series, the instruction sent by the control unit is the flow going through the specific storage.